

# 000 001 002 003 004 005 AHA! ANIMATING HUMAN AVATARS IN DIVERSE 006 SCENES WITH GAUSSIAN SPLATTING 007 008 009

010 **Anonymous authors**  
011 Paper under double-blind review  
012  
013  
014  
015  
016  
017  
018  
019  
020  
021  
022



023 Figure 1. We extend 3D Gaussian splatting to human animation, introducing a unified Gaussian-based  
024 representation for both humans and environments. This enables dynamic synthesis of human–scene interactions  
025 and photorealistic rendering with the Gaussian splatting algorithm, demonstrating a new direction for neural  
026 scene representations in animation.

## 027 ABSTRACT 028

029 We present a novel framework for animating humans in 3D scenes using 3D Gaus-  
030 sian Splatting (3DGS), a neural scene representation that has recently achieved  
031 state-of-the-art photorealistic results for novel-view synthesis but remains under-  
032 explored for human–scene animation and interaction. Unlike existing animation  
033 pipelines that use meshes or point clouds as the underlying 3D representation, our  
034 approach introduces the use of 3DGS as the 3D representation to the problem of  
035 animating humans in scenes. By representing humans and scenes as Gaussians,  
036 our approach allows for geometry-consistent free-viewpoint rendering of humans  
037 interacting with 3D scenes. Our key insight is that the rendering can be decoupled  
038 from the motion synthesis and each sub-problem can be addressed independently,  
039 without the need for paired human–scene data. Central to our method is a Gaussian-  
040 aligned motion module that synthesizes motion without explicit scene geometry,  
041 using opacity-based cues and projected Gaussian structures to guide human place-  
042 ment and pose alignment. To ensure natural interactions, we further propose a  
043 human–scene Gaussian refinement optimization that enforces realistic contact and  
044 navigation. We evaluate our approach on scenes from Scannet++ and the Super-  
045 Splat library, and on avatars reconstructed from sparse and dense multi-view human  
046 capture. Finally, we demonstrate that our framework allows for novel applications  
047 such as geometry-consistent free-viewpoint rendering of edited monocular RGB  
048 videos with new animated humans, showcasing the unique advantage of 3DGS for  
049 monocular video-based human animation.

## 050 1 INTRODUCTION 051

052 Human animation in 3D scenes is essential for applications ranging from video gaming and computer-  
053 generated imagery (CGI) to robotics. Recent research has made significant progress on generating  
humans in 3D scenes (Hassan et al., 2019; Jiang et al., 2024a; Hassan et al., 2021b; Zhao et al., 2023;

054 Hwang et al., 2025), where humans are typically represented as either 3D skeletons or meshes, while  
 055 background scenes are represented as meshes or point clouds. These representations are compact and  
 056 versatile, capable of modeling a wide variety of surfaces. However, a fundamental limitation persists:  
 057 there is almost always a domain gap between rendered results and real images due to limitations in  
 058 lighting, materials, and geometric fidelity.

059 In parallel, neural scene representations have emerged, beginning with NeRF (Mildenhall et al., 2020)  
 060 and recently 3D Gaussian Splatting (Kerbl et al., 2023), enabling photorealistic rendering of objects,  
 061 humans, and full 3D scenes from novel viewpoints or in novel poses. Yet, despite their success in  
 062 rendering quality, neural representations have seen little to no adoption in human-scene animation  
 063 pipelines, which continue to rely on mesh and point cloud-based frameworks.

064 Gaussian Splatting as a 3D representation for human-scene animation, *in theory* offers natural  
 065 advantages over existing mesh based representations: First, 3DGS enables photorealistic rendering  
 066 of human-scene interactions with superior lighting and material fidelity. Second, 3DGS allows for  
 067 reconstructing scenes with only a monocular video (Ling et al., 2024) captured from a mobile phone,  
 068 thus allowing for applications such as geometry consistent free viewpoint rendering of videos with  
 069 new humans, personalized content creation and gaming in scenes from mobile-captured videos. Such  
 070 applications are difficult with a mesh based representation as estimating meshes, or pointclouds  
 071 from only monocular scene videos remains challenging (Wang et al., 2025). This motivates the  
 072 central question addressed in this paper: *Can neural scene representations—specifically Gaussian*  
 073 *Splatting—be effectively used as a 3D representation for human animation in 3D scenes?* (Fig. 1).

074 Several obstacles prevent a direct extension of 3DGS to human animation in 3D scenes. First, most  
 075 existing work on human–scene interaction synthesis (Hassan et al., 2021b; Jiang et al., 2024a; Hwang  
 076 et al., 2025; Zhao et al., 2023) assumes paired human motion data with scene geometry. Such  
 077 datasets are difficult to collect at scale, and conversion from mesh-based annotations into Gaussians is  
 078 non-trivial. Second, human–scene animation requires motion synthesis that respects both the structure  
 079 of the scene and the natural dynamics of the human pose, which for a non-mesh representation  
 080 remains non-trivial. Furthermore, unlike meshes, 3DGS does not provide explicit topology or clean  
 081 geometry, complicating tasks like surface-based contact modeling.

082 To address these challenges, we offer a novel perspective for human–scene animation, grounded in two  
 083 key insights: First, rendering of humans and scenes in 3DGS can be decoupled from motion synthesis.  
 084 That is, we can reconstruct humans and scenes independently, animate humans in a canonical space,  
 085 and then place them back into reconstructed 3DGS scenes. This is common in classical graphics  
 086 pipelines for meshes, where canonical models are animated via skinning or rigging, and has recently  
 087 been adopted for animatable 3DGS avatars as well. However, prior work has primarily studied such  
 088 Gaussian avatars in isolation. In contrast, our contribution is to extend this paradigm to human–scene  
 089 animation, where avatars must not only be animated but also consistently placed and rendered inside  
 090 reconstructed 3DGS scenes. Second, motion synthesis can itself be decoupled from explicit geometry:  
 091 even though 3DGS does not provide watertight surfaces, we show that its opacity fields and projected  
 092 Gaussian structures offer sufficient cues to guide human placement.

093 Our framework proceeds in two stages. First, we reconstruct humans as animatable Gaussians from  
 094 either multiview capture using an off-the-shelf module. These Gaussians are then posed using a  
 095 **Gaussian-aligned motion module** (Sec. 3.2), which computes scene-aligned motion parameters by  
 096 relying on opacity-based culling and orthographic projection of scene Gaussians for path finding.  
 097 Our core contribution is the migration and adaptation of traditional scene-mesh human interaction  
 098 techniques (including RL-based locomotion and motion transitions) to 3DGS. To further ensure  
 099 realistic interactions, we introduce a human–scene **Gaussian refinement optimization** (Sec. 3.3)  
 100 that adjusts the placement and motion of humans for natural contact and navigation within the scene.

101 To showcase the applicability of our method on diverse datasets, we present results on scenes from the  
 102 Scannet++ dataset (Yeshwanth et al., 2023) and from scenes downloaded from the publicly available  
 103 SuperSplat 3DGS library (SuperSplat). To demonstrate the efficacy of our method on different Avatar  
 104 reconstruction datasets, we also showcase results on Avatars from the BEHAVE (Bhatnagar et al.,  
 105 2022) and Avatarrex datasets (Zheng et al., 2023). The results from BEHAVE demonstrate that our  
 106 method works on avatars reconstructed from sparse camera setups. We finally demonstrate the utility  
 107 of our presented framework for geometry consistent free viewpoint rendering of monocular videos

108 with new animated humans on several monocular videos from the DL3DV dataset (Ling et al., 2024),  
 109 showcasing the unique advantage of 3DGS for casual video-based human animation.  
 110

111 To summarize our contributions are as follows:

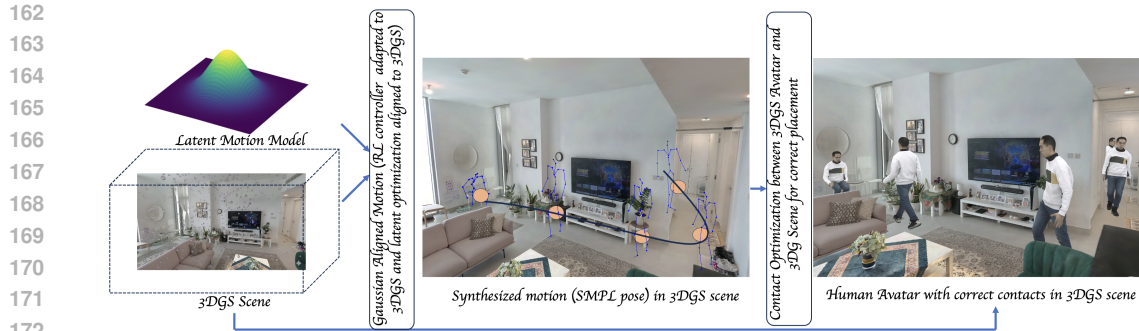
- 112 • We introduce the 3D Gaussian Splatting representation to the classical Computer Graphics  
 113 problem of animating humans in 3D environments
- 114 • We demonstrate that our framework can be used for geometry consistent free viewpoint  
 115 rendering of monocular videos edited with new animated humans
- 116 • We introduce a novel Gaussian aligned motion module for motion synthesis in scenes  
 117 represented as 3D Gaussians
- 118 • We introduce a human scene Gaussian refinement optimization for correct placement of hu-  
 119 man Gaussians in scenes represented using 3DGS leading to better contact and interactions.

## 122 2 RELATED WORK

123 **Neural Rendering** Following the publication of NeRF (Mildenhall et al., 2020), there has been  
 124 significant research on Neural Rendering (Xie et al., 2022b). Nerf is limited by its computational  
 125 complexity and despite several follow-up improvements (Müller et al., 2022; Barron et al., 2022;  
 126 2023; Tancik et al., 2023), the high computational cost of NeRF remain. 3DGS introduced in (Kerbl  
 127 et al., 2023) addresses this limitation by representing scenes with an explicit set of primitives shaped  
 128 as 3D Gaussians, extending previous work (Lassner & Zollhöfer, 2021). 3DGS rasterizes Gaussian  
 129 primitives into images using a splatting algorithm (Westover, 1992). 3DGS originally designed  
 130 for static scenes has been extended to dynamic scenes (Shaw et al., 2023; Luiten et al., 2024; Wu  
 131 et al., 2024; Lee et al., 2024; Li et al., 2023a), slam-based reconstruction, (Keetha et al., 2024),  
 132 mesh reconstruction (Huang et al., 2024; Guédon & Lepetit, 2024) and NVS from sparse cameras  
 133 (Mihajlovic et al., 2024).

134 **Human Reconstruction and Neural Rendering** Mesh-based templates (Pavlakos et al., 2019; Loper  
 135 et al., 2015) have been used to recover 3D human shape and pose from images and video (Bogo et al.,  
 136 2016; Kanazawa et al., 2018). However, this does not allow for photoreal renderings. In (Alldieck  
 137 et al.; 2019) recover a re-posable human avatar from monocular RGB. However their use of a mesh  
 138 template also does not allow for photorealistic renderings. Implicit functions (Mescheder et al., 2019;  
 139 Park et al., 2019) have also been utilized to reconstruct detailed 3D clothed humans (Chen et al.,  
 140 2021; Alldieck et al., 2021; Saito et al., 2020; He et al., 2021; Huang et al., 2020; Deng et al., 2020).  
 141 However, they are also unable to generate photorealistic renderings and are often not reposable.  
 142 Several works (Peng et al., 2021; Guo et al., 2023; Weng et al., 2022; Jiang et al., 2022; Habermann  
 143 et al., 2023; Zhu et al., 2024; Li et al., 2022; Liu et al., 2021; Xu et al., 2021) build a controllable  
 144 NeRF that produces photorealistic images of humans from input videos. Unlike us, they do not model  
 145 human-scene interactions. With the advent of 3DGS, several recent papers use a 3DGS formulation  
 146 (Kocabas et al., 2023; Qian et al., 2024; Moreau et al., 2024; Abdal et al., 2024; Zielonka et al.,  
 147 2023; Moon et al., 2024; Li et al., 2024b; Pang et al., 2024; Lei et al., 2023; Hu et al., 2024; Li et al.,  
 148 2024a; Zheng et al., 2024; Jiang et al., 2024b; Dhamo et al., 2024; Qian et al., 2023; Xu et al., 2024;  
 149 Junkawitsch et al., 2025) to build controllable human or face avatars. Unlike our method, they do not  
 150 model human-scene interactions. Prior works have also extended the 3DGS formulation to model  
 151 humans along with their environment, (Xue et al., 2024; Zhan et al., 2024; Mir et al., 2025), but  
 152 unlike us, they either do not focus on human animation in 3D scenes.

153 **Humans and Scenes** Human-scene interaction is a recurrent topic of study in computer vision and  
 154 graphics. Early works (Fouhey et al., 2014; Wang et al., 2017; Gupta et al., 2011) model affordances  
 155 and human-object interactions using monocular RGB. The collection of several recent human-scene  
 156 interaction datasets (Hassan et al., 2021a; Guzov et al., 2021; Hassan et al., 2019; Savva et al., 2016;  
 157 Taheri et al., 2020; Bhatnagar et al., 2022; Jiang et al., 2024a; Cheng et al., 2023; Zhang et al., 2022)  
 158 has allowed the computer vision community to make significant progress in joint 3D reconstruction  
 159 of human-object interactions (Xie et al., 2022a; 2023; 2024a; Zhang et al., 2020). These datasets have  
 160 also led to the development of methods that synthesize object conditioned controllable human motion  
 161 (Zhang et al., 2022; Starke et al., 2019b; Hassan et al., 2021c; Diller & Dai, 2024). All these methods  
 162 represent humans and scenes as 3D meshes and inherit the limitations of mesh-based representations



162  
163  
164  
165  
166  
167  
168  
169  
170  
171  
172  
173  
174  
175  
176  
177  
178  
179  
180  
181  
182  
183  
184  
185  
186  
187  
188  
189  
190  
191  
192  
193  
194  
195  
196  
197  
198  
199  
200  
201  
202  
203  
204  
205  
206  
207  
208  
209  
210  
211  
212  
213  
214  
215  
Figure 2: Using a latent motion model and 3DGS scene representation, we synthesize human motion that confirms with the 3D scene Gaussians using *Gaussian-aligned motion module*. We adapt RL based controllers and latent optimization for 3DGS scenes. We further refine these Gaussians for correct placements and contact. These composited human and scene Gaussians can be rendered from any viewpoint to generate photoal images.

including their inability to generate photorealistic images, while our method allows for photorealistic renderings of humans and scenes.

**Human Animation** Human animation is another extensively studied problem in vision and graphics. Motion matching (Reitsma & Pollard, 2007), learned motion matching (Clavet, 2016; Holden et al., 2020) and motion graphs (Lee et al., 2002; Fang & Pollard, 2003; Kovar et al., 2008; Safonova et al., 2004; Safonova & Hodgins, 2007) are common methods employed in the video-gaming industry for generating kinematic motion sequences. Deep learning variants (Holden et al., 2017; Starke et al., 2019a; 2021; 2020) have also gained popularity. Diffusion Models (Tevet et al., 2023) have emerged as a powerful paradigm for human motion synthesis. Several follow-up works extend the original Motion Diffusion model with physics(Yuan et al., 2023), blended-positional encoding (Barquero et al., 2024), and for fine-grained controllable motion synthesis (Karunratanakul et al., 2023; Pinyoanuntapong et al., 2024; Xie et al., 2024b). Reinforcement learning (Zhang & Tang, 2022; Zhao et al., 2023) is another oft-used paradigm used for motion synthesis. Diffusion models have also been used as latent-motion models (Zhao et al., 2025) but unlike us, they only focus on clean, noise-free mesh-based scene representations and ignore the rendering aspects of human-scene interaction leading to limited rendering quality and photorealism.

### 3 METHOD

We present a method that enables virtual humans represented using Gaussian splats to navigate and interact in complex environments reconstructed as 3D Gaussian scenes. Our framework consists of three key components: **(1) Gaussian Reconstruction:** We reconstruct both scenes and humans as 3D Gaussians from RGB images. For scenes, we use standard 3DGS reconstruction, while for humans, we learn *human Gaussian* representations that can be animated with different SMPL poses (Sec. 3.1). **(2) Gaussian-Aligned Motion Synthesis:** Central to our approach is a novel *Gaussian-aligned motion module* (Sec. 3.2), which uses the reconstructed scenes (Sec. 3.1) and a latent-variable based motion synthesis framework (using RL and latent space optimization adapted to 3DGS) to synthesize motion parameters aligned with the 3DGS scenes **(3) Differentiable Contact Refinement in 3DGS:** We use the synthesized human motion data to animate human Gaussians and apply a novel refinement algorithm for correct human-scene interaction (Sec. 3.3) (Fig. 3). The refinement module detects contact frames from motion data and optimizes translation vectors to enforce proper contact between human and scene Gaussians while maintaining temporal smoothness and avoiding penetrations. These composed Gaussians can be rendered from any camera viewpoint to produce videos of humans interacting with diverse scenes. Figure 2 provides an overview.

#### 3.1 GAUSSIAN RECONSTRUCTION

**Scene Gaussians.** Given monocular or multi-view video of a static scene, we model the environment as a set of  $N_S$  anisotropic 3D Gaussians  $\mathcal{G}^S = \{(\mu_i, \Sigma_i, \alpha_i, \mathbf{c}_i)\}_{i=1}^{N_S}$ , where each Gaussian has center  $\mu_i \in \mathbb{R}^3$ , covariance  $\Sigma_i \in \mathbb{R}^{3 \times 3}$ , opacity  $\alpha_i \in (0, 1)$ , and possibly view-dependent color  $\mathbf{c}_i$ .

Under the camera projection  $\Pi_t$ , each Gaussian projects to an ellipse with screen-space covariance  $\Sigma_{i,t}^{2D} = J_t \Sigma_i J_t^\top$ , where  $J_t = \frac{\partial \Pi_t}{\partial \mathbf{x}}|_{\mu_i}$  and  $\mathbf{u}_i = \Pi_t(\mu_i)$ . Its pixel contribution at  $\mathbf{u}$  is  $g_{i,t}(\mathbf{u}) = \exp(-\frac{1}{2}(\mathbf{u} - \mathbf{u}_i)^\top (\Sigma_{i,t}^{2D})^{-1}(\mathbf{u} - \mathbf{u}_i))$ , yielding effective opacity  $\hat{\alpha}_{i,t}(\mathbf{u}) = \alpha_i g_{i,t}(\mathbf{u})$ . The rendered image is obtained via front-to-back alpha compositing,

$$\hat{\mathbf{I}}_t(\mathbf{u}) = \sum_{i \in \mathcal{S}_t(\mathbf{u})} \left( \prod_{j \in \mathcal{S}_t(\mathbf{u}), j < i} (1 - \hat{\alpha}_{j,t}(\mathbf{u})) \right) \hat{\alpha}_{i,t}(\mathbf{u}) \mathbf{c}_i,$$

where  $\mathcal{S}_t(\mathbf{u})$  denotes the depth-sorted splats overlapping pixel  $\mathbf{u}$ . Parameters  $\Theta = \{\mu_i, \Sigma_i, \alpha_i, \mathbf{c}_i\}$  are optimized with the standard 3DGS photometric loss across frames.

**Human Gaussians.** We learn deformable human Gaussian representations from multi-view images that can be animated with different SMPL poses. Our approach consists of three key steps:

*Step 1: Canonical Gaussian parameterization on SMPL.* Given multi-view images of a person performing diverse poses, we learn a mapping from SMPL poses to 3D Gaussians in posed space. Following (Li et al., 2023b), we place Gaussians on the 2D manifold of the SMPL surface by constructing an approximate front–back UV atlas via orthographic projections of the SMPL mesh. Let  $\beta$  denote SMPL shape and  $\theta_t$  the pose at time  $t$ . We rasterize pose-conditioned features into a *pose map*  $P_t \in \mathbb{R}^{H \times W \times C}$  - denoted using  $\mathcal{M}(\beta, \theta_t)$ . A per-identity StyleUNet  $f_\phi$  predicts a set of *canonical* human Gaussians anchored on the SMPL surface:  $\mathcal{G}_t^C = f_\phi(P_t) = \{(\mathbf{x}_k^C, \Sigma_k^C, \mathbf{c}_k, \alpha_k)\}_{k=1}^{N_H}$ .

*Step 2: Skinning to posed space (LBS).* We obtain *posed* Gaussians by applying linear blend skinning (LBS) to canonical Gaussians  $\mathcal{G}_t^C$  with SMPL joint transformations  $\{(\mathbf{R}_b(\theta_t), \mathbf{t}_b(\theta_t))\}_{b=1}^B$  and vertex/bone weights  $w_{kb}$  inherited from the SMPL surface by using nearest neighbour sampling from Canonical Gaussians to SMPL vertices. With  $\mathcal{G}_t^P = \{(\mathbf{x}_k^P, \Sigma_k^P, \alpha_k, \mathbf{c}_k)\}_{k=1}^{N_H}$  we denote the posed human Gaussians at time  $t$ . During training, we render these posed Gaussians using standard 3DGS and supervise using multi-view images and cameras.

*Step 3: Pose-to-Gaussian inference (test-time).* Following (Li et al., 2023b), we compute the top  $K \in [10, 20]$  PCA components of training pose maps  $\{P_t\}$ , yielding mean  $\bar{P}$  and basis  $Q_K$ . At inference, poses synthesized by our Gaussian-aligned motion module (Sec. 3.2) are first projected to this subspace and then mapped to posed Gaussians:  $\hat{P}_y = \bar{P} + Q_K z_y$     $\mathcal{G}_y^P = \text{LBS}_{\theta_y}(f_\phi(\pi(\mathcal{M}(\beta, \theta_y))))$ . Here we use  $\pi$  to denote the projection to the subspace operation and  $y$  to indicate a test-time pose. For further details please see supplementary materials.

### 3.2 GAUSSIAN-ALIGNED MOTION SYNTHESIS

We introduce a Gaussian-aligned motion module that synthesizes controllable human motion directly in 3DGS scenes. Our key novelty is twofold: (i) we deploy reinforcement learning (RL) in Gaussian space by deriving reliable scene cues from opacity-weighted projections (no meshes or paired human–scene data required); and (ii) we couple RL locomotion with a deterministic latent optimizer for precise, contact-sensitive transitions in 3DGS scenes.

**Design overview.** We reuse a strong latent motion backbone trained on large scale mocap dataset and add two 3DGS-specific controllers: an RL locomotion policy that navigates between waypoints while avoiding scene Gaussians, and a deterministic latent-space optimizer that executes short, fine-grained actions near targets (e.g., stop, sit, grasp) before returning control to RL. While this explicit decomposition is not typical in existing motion synthesis frameworks, we find it especially effective in 3DGS settings, as this allows us to exploit the fact that in 3DGS scenes much of the raw scene detail can be abstracted to (i) a set of *paths* for navigation and (ii) *action points* (e.g., sitting locations, grasping targets provided by an animator) at which specific behaviors are executed - thus allowing for scene-aware motion synthesis without human–scene paired data. Both submodules operate consistently in the latent space of a learned motion model (Zhao et al., 2025).

**Latent motion backbone.** We adopt a latent motion prior, following prior work (Zhao et al., 2025) trained on AMASS (Punnakkal et al., 2021; Mahmood et al., 2019). Specifically, the model learns a compact motion-primitive space with a transformer VAE trained on mocap data, and places a diffusion prior in this latent space. Given motion history  $\mathbf{H}$  and a future motion segment  $\mathbf{X}$ , the encoder  $\mathcal{E}$  outputs a Gaussian posterior  $q_\phi(\mathbf{z} \mid \mathbf{H}, \mathbf{X}) = \mathcal{N}(\mu, \sigma^2 \mathbf{I})$  with reparameterized sample  $\mathbf{z} = \mu + \sigma \odot \varepsilon$  where  $\varepsilon \sim \mathcal{N}(\mathbf{0}, \mathbf{I})$ . The decoder  $\mathcal{D}$  reconstructs motion as  $\hat{\mathbf{X}} = \mathcal{D}(\mathbf{H}, \mathbf{z})$ . On this

270 latent space, a denoiser  $\mathcal{G}$  operates with forward process  
 271

$$q(\mathbf{z}_\tau \mid \mathbf{z}_{\tau-1}) = \mathcal{N}(\sqrt{1 - \beta_\tau} \mathbf{z}_{\tau-1}, \beta_\tau \mathbf{I})$$

272 and predicts the clean code  $\widehat{\mathbf{z}}_0 = \mathcal{G}(\mathbf{z}_\tau, \tau, \mathbf{H}, \mathbf{c})$ , where  $\mathbf{c}$  is an optional text embedding. During  
 273 inference we sample  $\mathbf{z}_{\tau_{\max}} \sim \mathcal{N}(\mathbf{0}, \mathbf{I})$ , perform about  $\tau_{\max} \approx 10$  denoising steps to obtain  $\widehat{\mathbf{z}}_0$ , decode  
 274  $\widehat{\mathbf{X}} = \mathcal{D}(\mathbf{H}, \widehat{\mathbf{z}}_0)$ , and update  $\mathbf{H}$  with the last  $H$  frames for autoregressive sampling. This latent  
 275 backbone is reused; our contribution lies in coupling it with 3DGS-specific controllers.  
 276

277 **Scene-adapted RL locomotion in 3DGS.** Our insight here is that locomotion policies trained in  
 278 mesh-based synthetic environments (Zhao et al., 2023) can be used in 3DGS reconstructions when  
 279 combined with our scene adaptation. We cast navigation as an MDP whose *action space* is the latent  
 280 space of the motion model. The policy outputs a start-noise  $\mathbf{z}_{\text{RL},i}^{(\tau_{\max})}$ , which a frozen  $\mathcal{G}, \mathcal{D}$  map to a  
 281 short motion clip, ensuring stable rollouts. At step  $i$ , the agent observes state  $s_i = (\mathbf{H}_i, \mathbf{g}_i, \boldsymbol{\eta}_i, \mathbf{c}_i)$   
 282 where  $\mathbf{H}_i$  is motion history,  $\mathbf{g}_i$  a goal cue,  $\boldsymbol{\eta}_i$  a scene cue, and  $\mathbf{c}_i$  a text embedding. The policy  
 283 samples  $a_i \sim \pi_\theta(\cdot \mid s_i)$ , interpreted as  $\mathbf{z}_{\text{RL},i}^{(\tau_{\max})}$ . The resulting clip  $\mathbf{X}_i$  updates the history  $\mathbf{H}_{i+1}$ .  
 284 Rewards  $r_i = r(s_i, a_i, s_{i+1})$  encourage waypoint progress, obstacle avoidance, and kinematic  
 285 plausibility. Training follows synthetic mesh-based environments as in (Zhao et al., 2023), while our  
 286 contribution is the deployment in 3DGS. For deployment in 3DGS scenes (which lack meshes), we  
 287 approximate navigation regions via orthographic projection: (i) compute PCA of Gaussian centers to  
 288 align a top-down view, (ii) threshold opacities to filter floaters, (iii) render a binary map of obstacles  
 289 and run A\* for pathfinding. The policy consumes an egocentric occupancy grid/walkability map  
 290  $\mathcal{M} \in \{0, 1\}^{N \times N}$  centered on the agent. For each grid cell  $u$ , we compute its nearest-neighbor  
 291 distance  $d(u)$  to filtered Gaussians and mark  $\mathcal{M}(u) = 1$  if  $d(u) > \tau$ , else 0. Despite being  
 292 approximate, this provides sufficiently reliable local context for navigation in 3DGS scenes. For  
 293 inference during locomotion, we fix text cue  $\mathbf{c}_i$  to "walk". For details please see supp mat.  
 294

295 **Latent optimization for transitions in 3DGS.** Once the agent reaches the vicinity of an action point,  
 296 control switches from RL to *deterministic latent-space optimization* for fine-grained actions such as  
 297 stopping, sitting, or grasping. Following (Zhao et al., 2025), we adopt a deterministic DDIM sampler  
 298 (no step-skipping), which defines a fixed rollout (see supp. mat.)  $\mathbf{M} = \text{ROLLOUT}(\mathbf{Z}_{\text{opt}}, \mathbf{H}_{\text{seed}}, \mathbf{C})$ ,  
 299 where  $\mathbf{Z}_{\text{opt}}$  is the terminal noise variable,  $\mathbf{H}_{\text{seed}}$  the seed history, and  $\mathbf{C}$  a fixed text cue ("sit", "grab").  
 300 We optimize  $\mathbf{Z}_{\text{opt}}$  by minimizing

$$\mathcal{L}(\mathbf{Z}_{\text{opt}}) = F(\Pi(\mathbf{M}), \mathbf{g}_{\text{user}}) + \text{Cons}(\mathbf{M})$$

301 with gradient updates  $\mathbf{Z}_{\text{opt}}^{(k+1)} = \mathbf{Z}_{\text{opt}}^{(k)} - \eta \nabla_{\mathbf{Z}_{\text{opt}}} \mathcal{L}(\mathbf{Z}_{\text{opt}}^{(k)})$ , where  $\Pi(\cdot)$  projects the rollout onto task-  
 302 relevant variables,  $F$  measures goal satisfaction, and Cons adds continuity, collision, and smoothness  
 303 constraints.

304 For position-only goals  $\mathbf{g}_{\text{user}}$  (e.g., sitting or grabbing at a user-provided point), we synthesize a short  
 305  $f$ -frame snippet  $\mathbf{M} = (\mathbf{M}_1, \dots, \mathbf{M}_f)$  starting from the locomotion end state  $\mathbf{M}_{\text{end}}^{\text{loc}}$ . In this setting,  $F$   
 306 corresponds to the reach and stop terms, with  $\mathcal{L}_{\text{reach}} = \|\mathbf{x}_f(j^*) - \mathbf{g}\|_2^2$  and  $\mathcal{L}_{\text{stop}} = \|\mathbf{v}_f(j^*)\|_2^2$ , while  
 307 Cons corresponds to start-continuity  $\mathcal{L}_{\text{start}} = \|\mathbf{M}_1 - \mathbf{M}_{\text{end}}^{\text{loc}}\|_2^2$ , collision  $\mathcal{L}_{\text{coll}} = \sum_{b \in \mathcal{B}_f} [-\phi(b)]_+^2$ ,  
 308 and smoothness  $\mathcal{L}_{\text{smooth}} = \frac{1}{f-1} \sum_{t=2}^f \|\mathbf{M}_t - \mathbf{M}_{t-1}\|_2^2$ . The final objective is therefore  
 309

$$\mathcal{L} = \mathcal{L}_{\text{reach}} + \lambda_v \mathcal{L}_{\text{stop}} + \lambda_{\text{start}} \mathcal{L}_{\text{start}} + \lambda_{\text{coll}} \mathcal{L}_{\text{coll}} + \lambda_s \mathcal{L}_{\text{smooth}}$$

310 Here  $j^*$  is an anchor joint (e.g., pelvis),  $\mathbf{x}_f, \mathbf{v}_f$  are its pose and velocity at frame  $f$ ,  $\mathcal{B}_f$  are sampled  
 311 SMPL points at frame  $f$ , and  $\phi(\cdot)$  is a differentiable signed-distance proxy to 3DGS Gaussians.  
 312 After completing the action, the same formulation synthesizes the exit transition (e.g., sit  $\rightarrow$  walk),  
 313 after which locomotion resumes. Though our method can synthesize actions which mimic "picking  
 314 up", or "grabbing" in the scene it cannot lift actual objects from the scene - as we assume that the  
 315 scene remains static throughout.

### 320 3.3 DIFFERENTIABLE CONTACT REFINEMENT IN 3DGS 321

322 After animating the reconstructed human Gaussians with synthesized human motion data (Sec. 3.2),  
 323 we place them into the reconstructed 3DGS scene. Here we want to highlight that we never use  
 324 the SMPL mesh. We use the "SMPL pose" (the joint angles of the 24 SMPL joints or the 54



Figure 3: With (left) and right (without) refinement of Gaussians

SMPL-X joints) - to drive the 3DGS avatar. A naive composition of posed human Gaussians with scene Gaussians often leads to floor/geometry penetration and inconsistent contacts. We introduce a contact-aware refinement that solves for small, physically meaningful translations of a sparse set of human Gaussians so that contacts are respected and penetrations are reduced. (Fig. 3)

We first note that mapping SMPL pose to 3D Gaussians is fundamentally different from mapping SMPL pose to 3D SMPL mesh. Mapping SMPL pose to a mesh is just a linear blend skinning operation that maps canonical SMPL mesh vertices to posed SMPL vertices - hence the SMPL pose can usually be easily optimized to maintain contact with the scene. This is not the case with 3D human Gaussians. Mapping SMPL pose to 3D human Gaussians involves a forward pass through the learnt network - and then applying LBS to the output Gaussians. If we were to optimize the SMPL pose for correct contact this would entail getting a gradient through the neural network that maps SMPL pose to 3D Gaussians - which would probably be difficult to converge. Instead we optimize per-Gaussian offsets as the Gaussians (after being output by the network) are already placed close enough to reasonable locations in the 3d scene; thus we can simply optimize per gaussian offsets - with heavy regularization for correct contact. We describe the setup in detail below.

**Setup.** Let the posed human Gaussians at time  $t$  be  $\mathcal{G}_t^P = \{(\mathbf{x}_k^P, \Sigma_k^P, \alpha_k, \mathbf{c}_k)\}_{k=1}^{N_H}$ , and the scene Gaussians be  $\mathcal{G}^S$ . Our goal is to refine a subset of the human Gaussians by per-frame translations  $\mathbf{T}_{k,t}$  to achieve (i) contact where appropriate and (ii) separation elsewhere.

**Contact detection and indexing.** From synthesized SMPL motion, we detect contact frames for a set of body joints using simple kinematic cues. For joint  $c$  with position  $\mathbf{p}_{c,t}$ , velocity  $\mathbf{v}_{c,t} = \mathbf{p}_{c,t} - \mathbf{p}_{c,t-1}$  and acceleration  $\mathbf{a}_{c,t} = \mathbf{v}_{c,t} - \mathbf{v}_{c,t-1}$ , a frame is marked as contact if  $\delta_{c,t} = (|v_{c,t}^y| < \tau_v) \wedge (a_{c,t}^y < \tau_a)$ , where  $y$  is the vertical axis. Because human Gaussian templates have identity-dependent counts and no global correspondence, we lift SMPL contact vertices  $V_c^{\text{SMPL}}$  (e.g., feet, hip) to the human Gaussians via nearest-neighbour search in the canonical space:  $i^* = \arg \min_k \|\mathbf{x}_k^C - \mathbf{u}\|_2$ ,  $\mathbf{u} \in V_c^{\text{SMPL}}$ . The resulting index set  $\mathcal{I}_c$  specifies which human Gaussians may be refined at contact.

**Scene proximity in Gaussian space.** We measure scene proximity using a soft nearest-neighbour distance to scene Gaussians

$$d_\beta(\mathbf{x}) = -\frac{1}{\beta} \log \left( \sum_{j=1}^{N_S} \exp(-\beta \|\mathbf{x} - \boldsymbol{\mu}_j\|) \right),$$

where  $\boldsymbol{\mu}_j$  are scene Gaussian centers and  $\beta$  controls softness. This provides stable gradients for contact/separation without requiring explicit meshes.

**Refinement objective.** For a contact Gaussian  $k \in \mathcal{I}_c$  at frame  $t$  with indicator  $\delta_{c,t}$ , we optimize a translation  $\mathbf{T}_{k,t}$  and update  $\tilde{\mathbf{x}}_{k,t}^P = \mathbf{x}_{k,t}^P + \mathbf{T}_{k,t}$  by minimizing

$$\mathbf{T}_{k,t}^* = \arg \min_{\mathbf{T}} \lambda_s \|\mathbf{x}_{k,t}^P + \mathbf{T} - \boldsymbol{\mu}_{j(k,t)}\|_2^2 + \lambda_d \psi(\mathbf{x}_{k,t}^P + \mathbf{T}, \delta_{c,t}) + \lambda_r \|\mathbf{T}\|_2^2,$$

where  $\boldsymbol{\mu}_{j(k,t)}$  is the nearest scene Gaussian center and

$$\psi(\mathbf{x}, \delta) = \begin{cases} d_\beta(\mathbf{x})^2, & \delta = 1 \text{ (enforce contact)} \\ h_r(d_\beta(\mathbf{x}))^2, & \delta = 0 \text{ (enforce separation)} \end{cases} \quad \text{with } h_r(d) = \max(0, r - d).$$



Figure 4: Qualitative results: Our method generates diverse motions across scenes and identities.

Table 1: **Evaluation design.** Two baselines  $\times$  two protocols. HQ: highest-quality rendering settings for each method. The same camera trajectories are used within each pairwise comparison.

Setting	Dataset / Source	3DGS Scene (ours)	Recons Mesh Scene (Baseline)	Baseline Rendering	Protocols
Baseline A	Mon. Vids (same scenes)	3DGS reconstruction	VGGT dense	3DGS	I and II
Baseline B	Replica and Curated	3DGS SuperSplat	Replica	Mesh	I and II

For temporal coherence, we add  $\lambda_t \sum_t \|\mathbf{T}_{k,t} - \mathbf{T}_{k,t-1}\|_2^2$ . Intuitively, the objective snaps designated contact Gaussians toward nearby scene surfaces when contact is detected, pushes them away otherwise, penalizes large displacements, and smooths motion over time.

The refined human Gaussians  $\tilde{\mathcal{G}}_t^P = \{(\tilde{\mathbf{x}}_{k,t}^P, \Sigma_k^P, \alpha_k, \mathbf{c}_k)\}_{k=1}^{N_H}$  are composed with  $\mathcal{G}^S$  and rendered with the standard 3DGS rasterizer to produce photorealistic interactions (e.g., walking, sitting) with improved contact fidelity and fewer penetrations. To the best of our knowledge, this is the first mesh-free refinement in Gaussian space that leverages a differentiable scene-distance, remains identity-agnostic via SMPL-to-Gaussian lifting, and operates as a lightweight post-hoc stage to improve contact realism without retraining.

## 4 EXPERIMENTS

For rendering evaluation, we present two modified mesh-based baselines (Baseline A and B) and evaluate with two evaluation protocols (I-human and II-automated). For further evaluation on motion quality and ablations please see the supplementary.

### 4.1 RENDERING EVALUATION

**Baseline A:** For Baseline A we collect monocular videos from DL3DV (Ling et al., 2024); each scene is reconstructed twice (once as 3DGS, once as a mesh using dense VGGT reconstruction (Wang et al., 2025)) so that comparisons are *within-scene*. Using the meshes obtained using dense VGGT reconstruction, we again use (Zhao et al., 2023) to generate SMPL-X parameters. Then we use these parameters naively to pose human Gaussians (Sec. 3.1) in the 3D scene and render the composited scene and human Gaussians using 3DGS. Note we do not perform any refinement. Furthermore note that the scene mesh is only used for motion synthesis but for rendering we use the 3DGS scene reconstruction and the posed human Gaussians. Baseline A is designed to show that a naive baseline that composites human and scenes Gaussians does not work out-of-the-box for monocular videos and hence provides further motivation for our algorithm. For baseline A evaluations, we render synchronized camera trajectories per pair (identical poses, FoV, and exposure).

**Baseline B:** In this experiment we aim to evaluate the rendering quality of a strong mesh-based baseline vs our 3DGS based algorithm. We use the highest quality existing mesh based 3D scenes from the Replica (Straub et al., 2019) dataset. In the Replica Scene we use the framework in (Zhao et al., 2023) to synthesize motion. Then we use a rigged scan from RenderPeople (along with its texture map) (RenderPeople) animated with the synthesized motion parameters in the Replica scene to generate the final renderings. For rendering our videos we use scenes from the Supersplat library and Avatars from Avatarrex (Zheng et al., 2023) dataset. This experiment aims to evaluate the highest

432  
433  
434  
435

Table 2: **Human preference study (win rate, %)** — fraction of pairwise trials where OURS is preferred. Baseline B compares OURS vs a mesh based baseline at highest-quality; Baseline A compares OURS (3DGS) vs a custom baseline designed for monocular videos. Higher is better.

	Replica vs 3DGS-Library (Baseline B)	Monocular (Baseline A)
OURS(3DGS) vs MESH	82.1	72.9

436  
437  
438  
439  
440  
441  
442  
443

Table 3: **VLM preference study (win rate, %)** — fraction of pairwise comparisons where OURS is preferred. Baseline B compares OURS vs a mesh based baseline at highest-quality; Baseline A compares OURS (3DGS) vs a custom baseline designed for monocular videos. Higher is better.

	Replica vs 3DGS-Library (Baseline B)	Monocular (Baseline A)
GPT-5	75.2	71.8
Gemini 2.5	69.1	65.9

444  
445  
446

quality rendering of a mesh based rendering vs a highest quality 3DGS renderings for the specific setting of human-scene animation. Note comparisons are not within scene.

447  
448  
449  
450  
451  
452  
453  
454  
455  
456  
457  
458  
459  
460

Here we want to highlight that finding the same scene+human combination for both our method and Baseline B would be difficult - because the data capture pipelines for 1) 3DGS vs mesh scene 2) 3DGS vs mesh human are fundamentally different. RenderPeople uses a rig of 250 DSLR cameras to capture a 3D human mesh - while the AvatarX dataset only uses 16 cameras and Behave dataset uses only 4. For 3DGS Avatar reconstruction motion of about 120 seconds inside the multiview camera setup is required while for a mesh capture only one frame is required. The way 3D scenes are reconstructed for Replica (mesh) and SuperSplat (3DGS) are also fundamentally - the replica reconstruction uses depth while some supersplat scenes use lidar. Additionally the replica original images are not available so we can't reconstruct a 3DGS splat for Replica scenes of the same quality as the ones on SuperSplat. As such for this particular baselines comparisons are not within scene.

461  
462  
463

We also want to acknowledge that for 3DGS animatable Avatars we require multiview video while a mesh can be reconstructed using multiview images. However we believe that for different use-cases, users would be willing to make the tradeoff for higher rendering quality.

464  
465  
466  
467  
468  
469

**Evaluation Protocol I: Human preference study** We conduct a pairwise *forced-choice* study measuring perceived photorealism. Each trial presents two *mute* videos from ours vs Baseline A or ours vs Baseline B. Participants select the video they find *more photorealistic*. We generate 5 samples for both comparisons and aggregate votes by comparison. We collect 21 participants for both Baseline A and B. We report *win rate (%)* of OURS over its comparator.

470  
471  
472  
473  
474  
475

**Evaluation Protocol II: VLM-based pairwise judgment** We use two strong vision–language model (VLM): GPT-5 (OpenAI, 2025) and Gemini2.5 (Comanici et al., 2025) as *paired comparators* between still renderings. For each video pair, we uniformly sample 10 frames per method, form matched pairs at the same timestamps, and query the VLM with “which image looks more photoreal?”. The VLM outputs a ternary judgment {Left wins, Right wins, Tie}; we compute a *VLM win rate* as the percentage of non-tied pairs favoring OURS. We randomize image order and prevent leakage by removing textual overlays and metadata.

476  
477  
478  
479

For the pairwise VLM study, the VLM is instructed to ignore artistic style and focus on physical plausibility: “which image looks more photoreal? Consider geometry (straight lines, depth cues), materials (BRDF, speculars), lighting/shadows, and absence of artifacts (flicker, halos, floaters).

480  
481  
482  
483  
484  
485

**Results Baseline A (Same monocular video)** On the within-scene comparison (Fig. 6), OURS outperforms the mesh baseline in both human and VLM judgments (Tables 2–3). Note that the scene meshes reconstructed using VGGT often exhibit blocky structures, blocked paths and hence are not suitable for motion synthesis, while our algorithm directly operates in Gaussian Space and doesn't suffer from the same problems. For detailed failure modes see Supp Mat.

**Baseline B (Replica Scene), HQ vs HQ.** Across both evaluations (Fig. 6) OURS is preferred by humans and by the VLM comparator (Tables 2–3) - thus clearly underscoring the central premise



Figure 5: Free viewpoint rendering of edited monocular video with animated humans



Figure 6: Visual Comparisons with Baselines

of the paper - *that neural scene representations yield better rendering quality for human-scene interaction* compared to existing mesh based representations.

## 4.2 QUALITATIVE RESULTS AND FREE VIEWPOINT RENDERING OF EDITED VIDEOS

In Fig. 4, we show results for diverse scenes from the SuperSplat library, Scannet scenes with Avatars from BEHAVE (sparse only 4 cameras), DNA-Rendering (Cheng et al., 2023), Avatarrex (Zheng et al., 2023) datasets. In Fig. 5, we demonstrate that our method works for monocular RGB scene videos and allows for free viewpoint rendering of videos edited with geometry consistent placement of animated humans in the scene. For more results please see the supplementary.

## 5 CONCLUSION

We have presented, to the best of our knowledge, the first method to synthesize human interactions in diverse 3D environments using 3D Gaussian Splatting (3DGS) as the underlying 3D representation. Our results suggest that neural rendering is now mature enough to function as a practical component in end-to-end 3D human–scene animation pipelines, bridging previously disjoint lines of work in human–scene animation and neural rendering. **Crucially, our pipeline operates on scenes reconstructed from monocular RGB video** and allows for applications such as monocular RGB geometry consistent video editing. We believe this framing and evidence open new research directions at the intersection of human animation, scene understanding, and neural rendering.

**Limitations.** Despite this progress, our pipeline has several limitations. First, complex and rapidly changing illumination can cause rendering artifacts and imperfect relighting. Second, we do not enforce full physics-based constraints, which can yield interactions that look plausible yet violate contact, stability, or momentum conservation. Third, the range of interaction types is limited; highly dexterous manipulation and long-horizon, multi-contact behaviors remain challenging. Fourth, we assume access to multiview videos of a human performing diverse actions.

**Outlook.** Addressing these issues suggests several promising research directions: integrating stronger lighting estimation and inverse rendering, incorporating differentiable or learned physics priors for contact and dynamics, expanding the interaction vocabulary to richer, longer, and multi-person scenarios and investigation how Avatars that generalize to Out-of-distribution poses can be reconstructed from monocular videos. We hope this work provides a foundation for scalable, video-native human–scene animation pipelines and catalyzes further advances in data, models, and evaluation for interactive 3D human animation.

540 REFERENCES  
541

542 Rameen Abdal, Wang Yifan, Zifan Shi, Yinghao Xu, Ryan Po, Zhengfei Kuang, Qifeng Chen,  
543 Dit-Yan Yeung, and Gordon Wetzstein. Gaussian shell maps for efficient 3d human generation. In  
544 *Proceedings of CVPR*, 2024.

545 Thiemo Alldieck, Marcus Magnor, Weipeng Xu, Christian Theobalt, and Gerard Pons-Moll. Video  
546 based reconstruction of 3d people models. In *IEEE Conference on Computer Vision and Pattern*  
547 *Recognition*. CVPR Spotlight Paper.

548 Thiemo Alldieck, Marcus Magnor, Bharat Lal Bhatnagar, Christian Theobalt, and Gerard Pons-Moll.  
549 Learning to reconstruct people in clothing from a single RGB camera. In *IEEE Conference on*  
550 *Computer Vision and Pattern Recognition (CVPR)*, jun 2019.

551 Thiemo Alldieck, Hongyi Xu, and Cristian Sminchisescu. imghum: Implicit generative models of 3d  
552 human shape and articulated pose. In *Proceedings of the IEEE/CVF International Conference on*  
553 *Computer Vision*, pp. 5461–5470, 2021.

554 German Barquero, Sergio Escalera, and Cristina Palmero. Seamless human motion composition with  
555 blended positional encodings. 2024.

556 Jonathan T Barron, Ben Mildenhall, Dor Verbin, Pratul P Srinivasan, and Peter Hedman. Mip-nerf  
557 360: Unbounded anti-aliased neural radiance fields. In *Proceedings of the IEEE/CVF conference*  
558 *on computer vision and pattern recognition*, pp. 5470–5479, 2022.

559 Jonathan T. Barron, Ben Mildenhall, Dor Verbin, Pratul P. Srinivasan, and Peter Hedman. Zip-nerf:  
560 Anti-aliased grid-based neural radiance fields. *ICCV*, 2023.

561 Bharat Lal Bhatnagar, Xianghui Xie, Ilya A Petrov, Cristian Sminchisescu, Christian Theobalt,  
562 and Gerard Pons-Moll. Behave: Dataset and method for tracking human object interactions.  
563 In *Proceedings of the IEEE/CVF Conference on Computer Vision and Pattern Recognition*, pp.  
564 15935–15946, 2022.

565 Federica Bogo, Angjoo Kanazawa, Christoph Lassner, Peter Gehler, Javier Romero, and Michael J.  
566 Black. Keep it SMPL: Automatic estimation of 3D human pose and shape from a single image.  
567 In *Computer Vision – ECCV 2016*, Lecture Notes in Computer Science. Springer International  
568 Publishing, October 2016.

569 Xu Chen, Yufeng Zheng, Michael J Black, Otmar Hilliges, and Andreas Geiger. Snarf: Differentiable  
570 forward skinning for animating non-rigid neural implicit shapes. In *International Conference on*  
571 *Computer Vision (ICCV)*, 2021.

572 Wei Cheng, Ruixiang Chen, Wanqi Yin, Siming Fan, Keyu Chen, Honglin He, Huiwen Luo, Zhongang  
573 Cai, Jingbo Wang, Yang Gao, Zhengming Yu, Zhengyu Lin, Daxuan Ren, Lei Yang, Ziwei Liu,  
574 Chen Change Loy, Chen Qian, Wayne Wu, Dahua Lin, Bo Dai, and Kwan-Yee Lin. Dna-rendering:  
575 A diverse neural actor repository for high-fidelity human-centric rendering. *arXiv preprint*,  
576 arXiv:2307.10173, 2023.

577 Simon Clavet. Motion matching and the road to next-gen animation. In *Game Development*  
578 *Conference*, 2016.

579 Gheorghe Comanici, Eric Bieber, ... Zach Gleicher, Thang Luong, and Niket Kumar Bhumihar.  
580 Gemini 2.5: Pushing the frontier with advanced reasoning, multimodality, long context, and next  
581 generation agentic capabilities, 2025. URL <https://arxiv.org/abs/2507.06261>.

582 Boyang Deng, John P Lewis, Timothy Jeruzalski, Gerard Pons-Moll, Geoffrey Hinton, Mohammad  
583 Norouzi, and Andrea Tagliasacchi. Nasa neural articulated shape approximation. In *Computer*  
584 *Vision–ECCV 2020: 16th European Conference, Glasgow, UK, August 23–28, 2020, Proceedings,*  
585 *Part VII 16*, pp. 612–628. Springer, 2020.

586 Helisa Dhamo, Yinyu Nie, Arthur Moreau, Jifei Song, Richard Shaw, Yiren Zhou, and Eduardo  
587 Pérez-Pellitero. Headgas: Real-time animatable head avatars via 3d gaussian splatting. *ECCV*,  
588 2024.

594 Christian Diller and Angela Dai. Cg-hoi: Contact-guided 3d human-object interaction generation. In  
 595 *Proc. Computer Vision and Pattern Recognition (CVPR), IEEE*, 2024.  
 596

597 Anthony C Fang and Nancy S Pollard. Efficient synthesis of physically valid human motion. *ACM*  
 598 *Transactions on Graphics (TOG)*, 22(3):417–426, 2003.

599 David F Fouhey, Vincent Delaitre, Abhinav Gupta, Alexei A Efros, Ivan Laptev, and Josef Sivic.  
 600 People watching: Human actions as a cue for single view geometry. *International journal of*  
 601 *computer vision*, 110(3):259–274, 2014.

602 Antoine Guédon and Vincent Lepetit. Sugar: Surface-aligned gaussian splatting for efficient 3d mesh  
 603 reconstruction and high-quality mesh rendering. *CVPR*, 2024.

604

605 Chen Guo, Tianjian Jiang, Xu Chen, Jie Song, and Otmar Hilliges. Vid2avatar: 3d avatar recon-  
 606 struction from videos in the wild via self-supervised scene decomposition. In *Proceedings of the*  
 607 *IEEE/CVF Conference on Computer Vision and Pattern Recognition (CVPR)*, June 2023.

608 Abhinav Gupta, Scott Satkin, Alexei A Efros, and Martial Hebert. From 3d scene geometry to human  
 609 workspace. In *CVPR 2011*, pp. 1961–1968. IEEE, 2011.

610

611 Vladimir Guzov, Aymen Mir, Torsten Sattler, and Gerard Pons-Moll. Human poseitioning system  
 612 (hps): 3d human pose estimation and self-localization in large scenes from body-mounted sensors.  
 613 In *IEEE Conference on Computer Vision and Pattern Recognition (CVPR)*. IEEE, jun 2021.

614 Marc Habermann, Lingjie Liu, Weipeng Xu, Gerard Pons-Moll, Michael Zollhoefer, and Christian  
 615 Theobalt. Hdhumans: A hybrid approach for high-fidelity digital humans. 6(3), aug 2023. doi:  
 616 10.1145/3606927. URL <https://doi.org/10.1145/3606927>.

617

618 Mohamed Hassan, Vasileios Choutas, Dimitrios Tzionas, and Michael J. Black. Resolving 3D human  
 619 pose ambiguities with 3D scene constraints. In *Proceedings International Conference on Computer*  
 620 *Vision*, pp. 2282–2292. IEEE, October 2019. URL <https://prox.is.tue.mpg.de>.

621 Mohamed Hassan, Duygu Ceylan, Ruben Villegas, Jun Saito, Jimei Yang, Yi Zhou, and Michael  
 622 Black. Stochastic Scene-Aware motion prediction. August 2021a.

623 Mohamed Hassan, Duygu Ceylan, Ruben Villegas, Jun Saito, Jimei Yang, Yi Zhou, and Michael  
 624 Black. Stochastic scene-aware motion prediction. In *Proceedings of the International Conference*  
 625 *on Computer Vision 2021*, October 2021b.

626 Mohamed Hassan, Partha Ghosh, Joachim Tesch, Dimitrios Tzionas, and Michael J. Black. Populating  
 627 3D scenes by learning human-scene interaction. In *IEEE/CVF Conf. on Computer Vision and*  
 628 *Pattern Recognition (CVPR)*, pp. 14708–14718, June 2021c.

629

630 Tong He, Yuanlu Xu, Shunsuke Saito, Stefano Soatto, and Tony Tung. Arch++: Animation-ready  
 631 clothed human reconstruction revisited. In *Proceedings of the IEEE/CVF international conference*  
 632 *on computer vision*, pp. 11046–11056, 2021.

633 Daniel Holden, Taku Komura, and Jun Saito. Phase-functioned neural networks for character control.  
 634 *ACM Transactions on Graphics (TOG)*, 36(4):1–13, 2017.

635

636 Daniel Holden, Oussama Kanoun, Maksym Perepichka, and Tiberiu Popa. Learned motion matching.  
 637 *ACM Transactions on Graphics (TOG)*, 39(4):53–1, 2020.

638

639 Liangxiao Hu, Hongwen Zhang, Yuxiang Zhang, Boyao Zhou, Boning Liu, Shengping Zhang, and  
 640 Liqiang Nie. Gaussianavatar: Towards realistic human avatar modeling from a single video via  
 641 animatable 3d gaussians. In *Proceedings of the IEEE/CVF conference on computer vision and*  
 642 *pattern recognition*, pp. 634–644, 2024.

643

644 Binbin Huang, Zehao Yu, Anpei Chen, Andreas Geiger, and Shenghua Gao. 2d gaussian splatting for  
 645 geometrically accurate radiance fields. In *SIGGRAPH 2024 Conference Papers*. Association for  
 646 Computing Machinery, 2024. doi: 10.1145/3641519.3657428.

647

Zeng Huang, Yuanlu Xu, Christoph Lassner, Hao Li, and Tony Tung. Arch: Animatable reconstruction  
 648 of clothed humans. In *Proceedings of the IEEE/CVF Conference on Computer Vision and Pattern*  
 649 *Recognition*, pp. 3093–3102, 2020.

648 Inwoo Hwang, Bing Zhou, Young Min Kim, Jian Wang, and Chuan Guo. Scenemi: Motion in-  
 649 betweening for modeling human-scene interactions, 2025. URL <https://arxiv.org/abs/2503.16289>.  
 650

651 Nan Jiang, Zhiyuan Zhang, Hongjie Li, Xiaoxuan Ma, Zan Wang, Yixin Chen, Tengyu Liu, Yixin  
 652 Zhu, and Siyuan Huang. Scaling up dynamic human-scene interaction modeling. In *Proceedings*  
 653 *of the IEEE/CVF Conference on Computer Vision and Pattern Recognition*, pp. 1737–1747, 2024a.  
 654

655 Wei Jiang, Kwang Moo Yi, Golnoosh Samei, Oncel Tuzel, and Anurag Ranjan. Neuman: Neural  
 656 human radiance field from a single video, 2022. URL <https://arxiv.org/abs/2203.12575>.  
 657

658 Yuheng Jiang, Zhehao Shen, Yu Hong, Chengcheng Guo, Yize Wu, Yingliang Zhang, Jingyi Yu, and  
 659 Lan Xu. Robust dual gaussian splatting for immersive human-centric volumetric videos. *arXiv*  
 660 *preprint arXiv:2409.08353*, 2024b.  
 661

662 Hendrik Junkawitsch, Guoxing Sun, Heming Zhu, Christian Theobalt, and Marc Habermann. Eva:  
 663 Expressive virtual avatars from multi-view videos. pp. 1–11, 2025.  
 664

665 Angjoo Kanazawa, Michael J. Black, David W. Jacobs, and Jitendra Malik. End-to-end recovery of  
 666 human shape and pose. In *Computer Vision and Pattern Recognition (CVPR)*, 2018.  
 667

668 Korrawe Karunratanakul, Konpat Preechakul, Emre Aksan, Thabo Beeler, Supasorn Suwa-  
 669 janakorn, and Siyu Tang. Optimizing diffusion noise can serve as universal motion priors. In  
 670 *arxiv:2312.11994*, 2023.  
 671

671 Nikhil Keetha, Jay Karhade, Krishna Murthy Jatavallabhula, Gengshan Yang, Sebastian Scherer,  
 672 Deva Ramanan, and Jonathon Luiten. Splatam: Splat, track & map 3d gaussians for dense rgb-d  
 673 slam. In *Proceedings of the IEEE/CVF Conference on Computer Vision and Pattern Recognition*,  
 674 2024.  
 675

675 Bernhard Kerbl, Georgios Kopanas, Thomas Leimkühler, and George Drettakis. 3d gaussian splatting  
 676 for real-time radiance field rendering. *ACM Transactions on Graphics*, 42(4), July 2023. URL  
 677 <https://repo-sam.inria.fr/fungraph/3d-gaussian-splatting/>.  
 678

679 Muhammed Kocabas, Jen-Hao Rick Chang, James Gabriel, Oncel Tuzel, and Anurag Ranjan. Hugs:  
 680 Human gaussian splats. *arXiv preprint arXiv:2311.17910*, 2023.  
 681

681 Lucas Kovar, Michael Gleicher, and Frédéric Pighin. Motion graphs. In *ACM SIGGRAPH 2008*  
 682 *classes*, pp. 1–10. 2008.  
 683

684 Christoph Lassner and Michael Zollhöfer. Pulsar: Efficient sphere-based neural rendering. In  
 685 *IEEE/CVF Conference on Computer Vision and Pattern Recognition (CVPR)*, June 2021.  
 686

687 Jehee Lee, Jinxiang Chai, Paul SA Reitsma, Jessica K Hodgins, and Nancy S Pollard. Interactive  
 688 control of avatars animated with human motion data. In *Proceedings of the 29th annual conference*  
 689 *on Computer graphics and interactive techniques*, pp. 491–500, 2002.  
 690

690 Junoh Lee, ChangYeon Won, Hyunjun Jung, Inhwan Bae, and Hae-Gon Jeon. Fully explicit dynamic  
 691 gaussian splatting. In *Proceedings of the Neural Information Processing Systems*, 2024.  
 692

692 Jiahui Lei, Yufu Wang, Georgios Pavlakos, Lingjie Liu, and Kostas Daniilidis. Gart: Gaussian  
 693 articulated template models. *arXiv preprint arXiv:2311.16099*, 2023.  
 694

695 Rui long Li, Julian Tanke, Minh Vo, Michael Zollhofer, Jurgen Gall, Angjoo Kanazawa, and Christoph  
 696 Lassner. Tava: Template-free animatable volumetric actors. In *European Conference on Computer*  
 697 *Vision (ECCV)*, 2022.  
 698

698 Zhan Li, Zhang Chen, Zhong Li, and Yi Xu. Spacetime gaussian feature splatting for real-time  
 699 dynamic view synthesis. *arXiv preprint arXiv:2312.16812*, 2023a.  
 700

701 Zhe Li, Zerong Zheng, Lizhen Wang, and Yebin Liu. Animatable gaussians: Learning pose-dependent  
 702 gaussian maps for high-fidelity human avatar modeling. *arXiv preprint arXiv:2311.16096*, 2023b.

702 Zhe Li, Yipengjing Sun, Zerong Zheng, Lizhen Wang, Shengping Zhang, and Yebin Liu. Animatable and relightable gaussians for high-fidelity human avatar modeling. *arXiv preprint arXiv:2311.16096v4*, 2024a.

703

704

705 Zhe Li, Zerong Zheng, Lizhen Wang, and Yebin Liu. Animatable gaussians: Learning pose-  
706 dependent gaussian maps for high-fidelity human avatar modeling. In *Proceedings of the IEEE/CVF  
707 Conference on Computer Vision and Pattern Recognition (CVPR)*, 2024b.

708

709 Lu Ling, Yichen Sheng, Zhi Tu, Wentian Zhao, Cheng Xin, Kun Wan, Lantao Yu, Qianyu Guo, Zixun  
710 Yu, Yawen Lu, et al. Dl3dv-10k: A large-scale scene dataset for deep learning-based 3d vision.  
711 In *Proceedings of the IEEE/CVF Conference on Computer Vision and Pattern Recognition*, pp.  
712 22160–22169, 2024.

713

714 Lingjie Liu, Marc Habermann, Viktor Rudnev, Kripasindhu Sarkar, Jiatao Gu, and Christian Theobalt.  
715 Neural actor: Neural free-view synthesis of human actors with pose control. *ACM Trans. Graph.(ACM SIGGRAPH Asia)*, 2021.

716

717 Matthew Loper, Naureen Mahmood, Javier Romero, Gerard Pons-Moll, and Michael J. Black. SMPL:  
718 A skinned multi-person linear model. *ACM Trans. Graphics (Proc. SIGGRAPH Asia)*, 34(6):  
719 248:1–248:16, October 2015. doi: 10.1145/2816795.2818013.

720

721 Jonathon Luiten, Georgios Kopanas, Bastian Leibe, and Deva Ramanan. Dynamic 3d gaussians:  
722 Tracking by persistent dynamic view synthesis. In *3DV*, 2024.

723

724 Naureen Mahmood, Nima Ghorbani, Nikolaus F. Troje, Gerard Pons-Moll, and Michael J. Black.  
725 AMASS: Archive of motion capture as surface shapes. In *International Conference on Computer  
Vision*, pp. 5442–5451, October 2019.

726

727 Lars Mescheder, Michael Oechsle, Michael Niemeyer, Sebastian Nowozin, and Andreas Geiger.  
728 Occupancy networks: Learning 3d reconstruction in function space. In *Proceedings of the  
IEEE/CVF conference on computer vision and pattern recognition*, pp. 4460–4470, 2019.

729

730 Marko Mihajlovic, Sergey Prokudin, Siyu Tang, Robert Maier, Federica Bogo, Tony Tung, and  
731 Edmond Boyer. SplatFields: Neural gaussian splats for sparse 3d and 4d reconstruction. In  
732 *European Conference on Computer Vision (ECCV)*. Springer, 2024.

733

734 Ben Mildenhall, Pratul P. Srinivasan, Matthew Tancik, Jonathan T. Barron, Ravi Ramamoorthi, and  
735 Ren Ng. Nerf: Representing scenes as neural radiance fields for view synthesis. In *ECCV*, 2020.

736

737 Aymen Mir, Arthur Moreau, Helisa Dhamo, Zhensong Zhang, and Eduardo Pérez-Pellitero. Gaspacho:  
738 Gaussian splatting for controllable humans and objects, 2025. URL <https://arxiv.org/abs/2503.09342>.

739

740 Gyeongsik Moon, Takaaki Shiratori, and Shunsuke Saito. Expressive whole-body 3D gaussian avatar.  
741 In *ECCV*, 2024.

742

743 Arthur Moreau, Jifei Song, Helisa Dhamo, Richard Shaw, Yiren Zhou, and Eduardo Pérez-Pellitero.  
744 Human gaussian splatting: Real-time rendering of animatable avatars. In *Proceedings of the  
IEEE/CVF Conference on Computer Vision and Pattern Recognition*, pp. 788–798, 2024.

745

746 Thomas Müller, Alex Evans, Christoph Schied, and Alexander Keller. Instant neural graphics primitives  
747 with a multiresolution hash encoding. *ACM Trans. Graph.*, 41(4):102:1–102:15, July 2022.  
748 doi: 10.1145/3528223.3530127. URL <https://doi.org/10.1145/3528223.3530127>.

749

750 OpenAI. Chatgpt (gpt-5). <https://chat.openai.com/>, 2025. Large language model, Septem-  
751 ber 2025 version.

752

753 Haokai Pang, Heming Zhu, Adam Kortylewski, Christian Theobalt, and Marc Habermann. Ash:  
754 Animatable gaussian splats for efficient and photoreal human rendering. In *Proceedings of the  
IEEE/CVF Conference on Computer Vision and Pattern Recognition*, pp. 1165–1175, 2024.

755

756 Jeong Joon Park, Peter Florence, Julian Straub, Richard Newcombe, and Steven Lovegrove. DeepSDF:  
757 Learning continuous signed distance functions for shape representation. In *Proceedings of the  
IEEE/CVF conference on computer vision and pattern recognition*, pp. 165–174, 2019.

756 Georgios Pavlakos, Vasileios Choutas, Nima Ghorbani, Timo Bolkart, Ahmed A. A. Osman, Dimitrios  
 757 Tzionas, and Michael J. Black. Expressive body capture: 3D hands, face, and body from a single  
 758 image. In *Proceedings IEEE Conf. on Computer Vision and Pattern Recognition (CVPR)*, pp.  
 759 10975–10985, 2019.

760 Sida Peng, Junting Dong, Qianqian Wang, Shangzhan Zhang, Qing Shuai, Xiaowei Zhou, and Hujun  
 761 Bao. Animatable neural radiance fields for modeling dynamic human bodies. In *ICCV*, 2021.

762 Ekkasit Pinyoanuntapong, Muhammad Usama Saleem, Korrawe Karunratanakul, Pu Wang, Hongfei  
 763 Xue, Chen Chen, Chuan Guo, Junli Cao, Jian Ren, and Sergey Tulyakov. Controlmm: Controllable  
 764 masked motion generation. *arXiv preprint arXiv:2410.10780*, 2024.

765 Abhinanda R. Punnakkal, Arjun Chandrasekaran, Nikos Athanasiou, Alejandra Quiros-Ramirez,  
 766 and Michael J. Black. BABEL: Bodies, action and behavior with english labels. In *Proceedings  
 767 IEEE/CVF Conf. on Computer Vision and Pattern Recognition (CVPR)*, pp. 722–731, June 2021.

768 Zhiyin Qian, Shaofei Wang, Marko Mihajlovic, Andreas Geiger, and Siyu Tang. 3dgs-avatar:  
 769 Animatable avatars via deformable 3d gaussian splatting. *arXiv preprint arXiv:2312.09228*, 2023.

770 Zhiyin Qian, Shaofei Wang, Marko Mihajlovic, Andreas Geiger, and Siyu Tang. 3dgs-avatar:  
 771 Animatable avatars via deformable 3d gaussian splatting. 2024.

772 Paul SA Reitsma and Nancy S Pollard. Evaluating motion graphs for character animation. *ACM  
 773 Transactions on Graphics (TOG)*, 26(4):18–es, 2007.

774 RenderPeople. Renderpeople. <https://renderpeople.com/>. Accessed: 2025-09-17.

775 Alla Safonova and Jessica K. Hodgins. Construction and optimal search of interpolated motion  
 776 graphs. *ACM Transactions on Graphics (SIGGRAPH 2007)*, 26(3), August 2007.

777 Alla Safonova, Jessica K Hodgins, and Nancy S Pollard. Synthesizing physically realistic human  
 778 motion in low-dimensional, behavior-specific spaces. *ACM Transactions on Graphics (ToG)*, 23  
 779 (3):514–521, 2004.

780 Shunsuke Saito, Tomas Simon, Jason Saragih, and Hanbyul Joo. Pifuhd: Multi-level pixel-aligned  
 781 implicit function for high-resolution 3d human digitization. In *CVPR*, 2020.

782 Manolis Savva, Angel X. Chang, Pat Hanrahan, Matthew Fisher, and Matthias Nießner. PiGraphs:  
 783 Learning Interaction Snapshots from Observations. *ACM Transactions on Graphics (TOG)*, 35(4),  
 784 2016.

785 Richard Shaw, Jifei Song, Arthur Moreau, Michal Nazarczuk, Sibi Catley-Chandar, Helisa Dhamo,  
 786 and Eduardo Perez-Pellitero. Swags: Sampling windows adaptively for dynamic 3d gaussian  
 787 splatting. *arXiv preprint arXiv:2312.13308*, 2023.

788 Sebastian Starke, He Zhang, Taku Komura, and Jun Saito. Neural state machine for character-scene  
 789 interactions. *ACM Trans. Graph.*, 38(6), November 2019a. ISSN 0730-0301.

790 Sebastian Starke, He Zhang, Taku Komura, and Jun Saito. Neural state machine for character-scene  
 791 interactions. *ACM Trans. Graph.*, 38(6), November 2019b. ISSN 0730-0301. doi: 10.1145/  
 792 3355089.3356505. URL <https://doi.org/10.1145/3355089.3356505>.

793 Sebastian Starke, Yiwei Zhao, Taku Komura, and Kazi Zaman. Local motion phases for learning  
 794 multi-contact character movements. *ACM Trans. Graph.*, 39(4), July 2020.

795 Sebastian Starke, Yiwei Zhao, Fabio Zinno, and Taku Komura. Neural animation layering for  
 796 synthesizing martial arts movements. *ACM Trans. Graph.*, 40(4), July 2021.

797 Julian Straub, Thomas Whelan, Lingni Ma, Yufan Chen, Erik Wijmans, Simon Green, Jakob J. Engel,  
 798 Raul Mur-Artal, Carl Ren, Shobhit Verma, Anton Clarkson, Mingfei Yan, Brian Budge, Yajie Yan,  
 799 Xiaqing Pan, June Yon, Yuyang Zou, Kimberly Leon, Nigel Carter, Jesus Briales, Tyler Gillingham,  
 800 Elias Mueggler, Luis Pesqueira, Manolis Savva, Dhruv Batra, Hauke M. Strasdat, Renzo De Nardi,  
 801 Michael Goesele, Steven Lovegrove, and Richard Newcombe. The Replica dataset: A digital  
 802 replica of indoor spaces. *arXiv preprint arXiv:1906.05797*, 2019.

810 SuperSplat. Supersplat. <https://superspl.at/>. Accessed: 2025-09-17.  
 811

812 Omid Taheri, Nima Ghorbani, Michael J. Black, and Dimitrios Tzionas. GRAB: A dataset of whole-  
 813 body human grasping of objects. In *European Conference on Computer Vision (ECCV)*, 2020.  
 814 URL <https://grab.is.tue.mpg.de>.

815 Matthew Tancik, Ethan Weber, Evonne Ng, Ruilong Li, Brent Yi, Justin Kerr, Terrance Wang,  
 816 Alexander Kristoffersen, Jake Austin, Kamyar Salahi, Abhik Ahuja, David McAllister, and Angjoo  
 817 Kanazawa. Nerfstudio: A modular framework for neural radiance field development. In *ACM  
 818 SIGGRAPH 2023 Conference Proceedings*, SIGGRAPH '23, 2023.

819 Guy Tevet, Sigal Raab, Brian Gordon, Yoni Shafir, Daniel Cohen-or, and Amit Haim Bermano.  
 820 Human motion diffusion model. In *The Eleventh International Conference on Learning Representations*, 2023. URL <https://openreview.net/forum?id=SJ1kSy02jwu>.  
 821

822 Jianyuan Wang, Minghao Chen, Nikita Karaev, Andrea Vedaldi, Christian Rupprecht, and David  
 823 Novotny. Vggt: Visual geometry grounded transformer. In *Proceedings of the IEEE/CVF  
 824 Conference on Computer Vision and Pattern Recognition*, 2025.

825 Xiaolong Wang, Rohit Girdhar, and Abhinav Gupta. Binge watching: Scaling affordance learning  
 826 from sitcoms. In *Proceedings of the IEEE Conference on Computer Vision and Pattern Recognition*,  
 827 pp. 2596–2605, 2017.

828 Chung-Yi Weng, Brian Curless, Pratul P. Srinivasan, Jonathan T. Barron, and Ira Kemelmacher-  
 829 Shlizerman. HumanNeRF: Free-viewpoint rendering of moving people from monocular video. In  
 830 *Proceedings of the IEEE/CVF Conference on Computer Vision and Pattern Recognition (CVPR)*,  
 831 pp. 16210–16220, June 2022.

832 Lee Alan Westover. *Splatting: a parallel, feed-forward volume rendering algorithm*. PhD thesis,  
 833 USA, 1992.

834 Guanjun Wu, Taoran Yi, Jiemin Fang, Lingxi Xie, Xiaopeng Zhang, Wei Wei, Wenyu Liu, Qi Tian,  
 835 and Xinggang Wang. 4d gaussian splatting for real-time dynamic scene rendering. In *Proceedings  
 836 of the IEEE/CVF Conference on Computer Vision and Pattern Recognition (CVPR)*, pp. 20310–  
 837 20320, June 2024.

838 Xianghui Xie, Bharat Lal Bhatnagar, and Gerard Pons-Moll. Chore: Contact, human and object  
 839 reconstruction from a single rgb image. In *European Conference on Computer Vision (ECCV)*.  
 840 Springer, October 2022a.

841 Xianghui Xie, Bharat Lal Bhatnagar, and Gerard Pons-Moll. Visibility aware human-object interaction  
 842 tracking from single rgb camera. In *IEEE Conference on Computer Vision and Pattern Recognition  
 843 (CVPR)*, June 2023.

844 Xianghui Xie, Bharat Lal Bhatnagar, Jan Eric Lenssen, and Gerard Pons-Moll. Template free  
 845 reconstruction of human-object interaction with procedural interaction generation. In *Proceedings  
 846 of the IEEE/CVF Conference on Computer Vision and Pattern Recognition*, pp. 10003–10015,  
 847 2024a.

848 Yiheng Xie, Towaki Takikawa, Shunsuke Saito, Or Litany, Shiqin Yan, Numair Khan, Federico  
 849 Tombari, James Tompkin, Vincent Sitzmann, and Srinath Sridhar. Neural fields in visual computing  
 850 and beyond. *Computer Graphics Forum*, 2022b. ISSN 1467-8659. doi: 10.1111/cgf.14505.

851 Yiming Xie, Varun Jampani, Lei Zhong, Deqing Sun, and Huaizu Jiang. Omnicontrol: Control any  
 852 joint at any time for human motion generation. In *The Twelfth International Conference on Learning  
 853 Representations*, 2024b. URL <https://openreview.net/forum?id=gd01AEtWso>.

854 Hongyi Xu, Thieno Alldieck, and Cristian Sminchisescu. H-nerf: Neural radiance fields for rendering  
 855 and temporal reconstruction of humans in motion. *Advances in Neural Information Processing  
 856 Systems*, 34:14955–14966, 2021.

857 Yuelang Xu, Benwang Chen, Zhe Li, Hongwen Zhang, Lizhen Wang, Zerong Zheng, and Yebin Liu.  
 858 Gaussian head avatar: Ultra high-fidelity head avatar via dynamic gaussians. In *Proceedings of the  
 859 IEEE/CVF Conference on Computer Vision and Pattern Recognition*, pp. 1931–1941, 2024.

864 Lixin Xue, Chen Guo, Chengwei Zheng, Fangjinhua Wang, Tianjian Jiang, Hsuan-I Ho, Manuel  
 865 Kaufmann, Jie Song, and Hilliges Otmar. HSR: holistic 3d human-scene reconstruction from  
 866 monocular videos. In *European Conference on Computer Vision (ECCV)*, 2024.

867 Chandan Yeshwanth, Yueh-Cheng Liu, Matthias Nießner, and Angela Dai. Scannet++: A high-fidelity  
 868 dataset of 3d indoor scenes. In *Proceedings of the International Conference on Computer Vision  
 869 (ICCV)*, 2023.

870 Ye Yuan, Jiaming Song, Umar Iqbal, Arash Vahdat, and Jan Kautz. Physdiff: Physics-guided human  
 871 motion diffusion model. In *Proceedings of the IEEE/CVF international conference on computer  
 872 vision*, pp. 16010–16021, 2023.

873 Yifan Zhan, Qingtian Zhu, Muyao Niu, Mingze Ma, Jiancheng Zhao, Zhihang Zhong, Xiao Sun,  
 874 Yu Qiao, and Yinqiang Zheng. Tomie: Towards modular growth in enhanced smpl skeleton for 3d  
 875 human with animatable garments, 2024. URL <https://arxiv.org/abs/2410.08082>.

876 Jason Y. Zhang, Sam Pepose, Hanbyul Joo, Deva Ramanan, Jitendra Malik, and Angjoo Kanazawa.  
 877 Perceiving 3d human-object spatial arrangements from a single image in the wild. In *European  
 878 Conference on Computer Vision (ECCV)*, 2020.

879 Xiaohan Zhang, Bharat Lal Bhatnagar, Sebastian Starke, Vladimir Guzov, and Gerard Pons-Moll.  
 880 Couch: Towards controllable human-chair interactions. *European Conference on Computer Vision  
 881 (ECCV)*, October 2022.

882 Yan Zhang and Siyu Tang. The wanderings of odysseus in 3d scenes. In *Proceedings of the IEEE/CVF  
 883 Conference on Computer Vision and Pattern Recognition*, pp. 20481–20491, 2022.

884 Kaifeng Zhao, Yan Zhang, Shaofei Wang, Thabo Beeler, and Siyu Tang. DIMOS: Synthesizing  
 885 diverse human motions in 3d indoor scenes. In *International conference on computer vision  
 886 (ICCV)*, 2023.

887 Kaifeng Zhao, Gen Li, and Siyu Tang. DartControl: A diffusion-based autoregressive motion model  
 888 for real-time text-driven motion control. In *The Thirteenth International Conference on Learning  
 889 Representations (ICLR)*, 2025.

890 Shunyuan Zheng, Boyao Zhou, Ruizhi Shao, Boning Liu, Shengping Zhang, Liqiang Nie, and Yebin  
 891 Liu. Gps-gaussian: Generalizable pixel-wise 3d gaussian splatting for real-time human novel  
 892 view synthesis. In *Proceedings of the IEEE/CVF Conference on Computer Vision and Pattern  
 893 Recognition (CVPR)*, 2024.

894 Zerong Zheng, Xiaochen Zhao, Hongwen Zhang, Boning Liu, and Yebin Liu. Avatarrex: Real-time  
 895 expressive full-body avatars. *ACM Transactions on Graphics (TOG)*, 42(4), 2023.

896 Heming Zhu, Fangneng Zhan, Christian Theobalt, and Marc Habermann. Trihuman: A real-time  
 897 and controllable tri-plane representation for detailed human geometry and appearance synthesis.  
 898 *ACM Trans. Graph.*, September 2024. ISSN 0730-0301. doi: 10.1145/3697140. URL <https://doi.org/10.1145/3697140>.

899 Wojciech Zienonka, Timur Bagautdinov, Shunsuke Saito, Michael Zollhöfer, Justus Thies, and Javier  
 900 Romero. Drivable 3d gaussian avatars. *arXiv preprint arXiv:2311.08581*, 2023.

901  
 902  
 903  
 904  
 905  
 906  
 907  
 908  
 909  
 910  
 911  
 912  
 913  
 914  
 915  
 916  
 917